Extension of generalized forced convective heat transfer coefficient expressions for isolated buildings taking into account oblique wind directions

Building and Environment 140 (2018) 194–208

Contents lists available at ScienceDirect

Building and Environment

journal homepage: www.elsevier.com/locate/buildenv

Extension of generalized forced convective heat transfer coefficient expressions for isolated buildings taking into account oblique wind directions

H. Montazeri[a,b,*], B. Blocken[a,b]

[a] Building Physics Section, Department of Civil Engineering, KU Leuven, Kasteelpark Arenberg 40 – bus 2447, 3001 Leuven, Belgium
[b] Building Physics and Services, Department of the Built Environment, Eindhoven University of Technology, P.O. box 513, 5600 MB Eindhoven, The Netherlands

ARTICLE INFO

Keywords:
Convective heat transfer coefficient
Computational Fluid Dynamics (CFD)
Building Energy Simulation (BES)
Building aerodynamics
Building energy

ABSTRACT

The surface-averaged forced Convective Heat Transfer Coefficient ($CHTC_{avg}$) at a windward building facade is influenced by the complex interaction between a wide range of parameters. Existing CHTC expressions, however, consider the impact of these parameters either incompletely or not at all. Earlier studies have shown that this shortcoming can lead to significant errors in Building Energy Simulations. In this paper, therefore, the combined impacts of wind speed (U_{10}), building height (H) and width (W), and wind direction (θ) on the $CHTC_{avg}$ for the windward facade of buildings are systematically investigated. High-resolution CFD simulations of wind flow and forced convective heat transfer, validated with wind-tunnel measurements, are performed for 64 building geometries (10 m ≤ H and W ≤ 80 m), 8 wind directions (0° ≤ θ ≤ 78.75°) and 4 reference wind speeds (1 m/s ≤ U_{10} ≤ 4 m/s). The 3D steady RANS equations with the realizable k-ε turbulence model and the low-Re number Wolfshtein model are used. The results show that for a given building geometry and U_{10}, the $CHTC_{avg}$ decreases as θ increases from 0° to 78.75°. The maximum reduction of about 42% occurs for the building with H = 8W = 80 m. In addition, for a given θ and U_{10}, by increasing H, the $CHTC_{avg}$ increases, while increasing W has the opposite impact on the $CHTC_{avg}$. Finally, a new generalized CHTC expression is presented as a function of U_{10}, H, W and θ, and its accuracy is confirmed by detailed in-sample and out-of-sample evaluations.

1. Introduction

Research and practice in urban physics, building energy and building component durability require the knowledge of the exterior forced convective heat transfer (CHT) at the building facades. For building energy studies, for example, the convective heat transfer coefficient (CHTC) is typically used to model the CHT between buildings and their environment as part of the calculation of the heating and cooling demand of buildings and to assess the energy performance of the building envelope. Knowledge of the CHTC is also important for modeling of heat waves in urban areas, the urban heat island effect, indoor and outdoor heat stress, etc., which are topics that are strongly related to the grand societal challenges energy, health and climate [1,2].

The CHTC distribution across the facades of a building is complex as it is influenced by a wide range of parameters including building geometry [3–6], wind speed [7–9] and wind direction [9–11], etc.

Earlier CFD studies have shown that the impact of building geometry on the forced CHTC can be very large and to some extent counter-intuitive [4,6]. For example, for a 10 m wide windward facade, as the building height (H) increases from 10 m to 80 m, the forced surface-averaged CHTC ($CHTC_{avg}$) on the windward facade increases by about 20% [4]. For H = 10 m, however, increasing the building width from 10 to 80 m has the opposite impact on the forced surface-averaged CHTC, which decreases by more than 33% [4]. The first trend can be explained by the increase of wind speed with height in the atmospheric boundary layer. The second trend is attributed to the so-called wind-blocking effect that refers to the upstream wind deceleration due to the blockage by the building [12,13].

Previous experimental and numerical studies have indicated that the forced CHTC changes as a function of Reynolds number. For example, a power-law dependence was found between the CHTC at the surfaces of wall-mounted rectangular prisms and the Reynolds number. For windward building facades, several power-law correlations between the $CHTC_{avg}$ and U_{10} have been provided (e.g., $CHTC = 5.15U_{10}^{0.81}$ [8], $CHTC = 4.6U_{10}^{0.89}$ [9], $CHTC = 5.01U_{10}^{0.85}$ [14]), where U_{10} is the mean wind speed in the undisturbed flow at a height of 10 m above the ground.

* Corresponding author. Building Physics Section, Department of Civil Engineering, KU Leuven, Leuven, Belgium.
E-mail address: hamid.montazeri@kuleuven.be (H. Montazeri).

https://doi.org/10.1016/j.buildenv.2018.05.027
Received 22 February 2018; Received in revised form 10 May 2018; Accepted 14 May 2018

The impact of wind direction on the CHTC was investigated in previous CFD studies (e.g. Refs. [8,9]). In each of these studies, only one specific low-rise isolated building was investigated while the simultaneous impact of building geometry was not taken into account. It was shown that the surface-averaged CHTC at the windward building facades varies substantially as a function of the wind direction. For example, Blocken et al. [9] showed that for a low-rise cubic building (10 m × 10 m × 10 m) and for U_{10} = 3 m, by increasing the wind direction from 0° to 78.75°, the $CHTC_{avg}$ reduces by more than 25%.

Because of the complexity involved in obtaining accurate values of the CHTC, a large number of empirical and semi-empirical expressions have been established using on-site (full-scale) measurements (e.g. the Mobile Window Thermal Test (MoWiTT) model [15], and the model by Liu and Harris [16]) or wind-tunnel (reduced-scale) measurements (e.g. the McAdams [17] and CIBS (Chartered Institute of Building Services) models [18]) as well as Computational Fluid Dynamics (CFD) simulations (e.g. the models by Emmel [8] and Montazeri & Blocken [6]). Many of these expressions are implemented in Building Energy Simulation (BES) programs [19,20]. However, the accuracy and reliability of these expressions are of concern because:

- Many of these expressions are based on invalid assumptions: an example is that the CHTC is often assumed constant across a building facade and that a measurement resulting from a single point is considered to be valid for the whole facade. Further, some expressions have been derived based on wind-tunnel measurements over a flat plate. For example, the McAdams [17] and CIBS models [18] that are widely used in BES tools have been derived based on wind-tunnel experiments for a vertical square copper plate (0.5 × 0.5 m^2) in a uniform air flow parallel to the plate [21]. The flow structure around buildings, however, is more complex than the one over flat plates.
- Generally, the influence of important parameters such as wind direction, surrounding buildings, and surface roughness is taken into account either incompletely, or not at all. In addition, a vast majority of these expressions do not contain the complex interaction between these parameters. An example is the correlation proposed in the CIBS Guide [18]: $CHTC = 4.1U_{loc} + 5.8$, where $U_{loc} = 2/3U_R$. In this correlation, U_{loc} is the wind speed at a certain distance from the building facade and at a certain height from the ground, and U_R is the wind speed at a certain height from the roof surface.
- Many expressions are case-specific, i.e., they were derived for specific building characteristics, and under specific meteorological conditions (wind speed and wind direction) and they are therefore strictly only applicable to the conditions for which they were derived. For example, the model by Liu & Harris [16] is based on full-scale measurements for a one-storey building in a rural area that is partially sheltered by a nearby building. The model provides three CHTC expressions based on U_{loc} ($CHTC = 6.31U_{loc} + 3.32$), U_R ($CHTC = 2.08U_R + 2.97$), and U_{10} ($CHTC = 1.53U_{10} + 1.43$), which were measured 0.5 m away from the wall surface, 1 m above the roof and 10 m above the ground level, respectively. Since a copper sheet (smooth surface) was used to measure the CHTC at the facades of this one-storey building, it is expected that this model is accurate only for low-rise buildings with smooth surfaces.

The accuracy of these empirical or semi-empirical expressions, so-called secondary sources, depends on availability and accuracy of the above-mentioned so-called primary sources, i.e., on-site or wind-tunnel experiments, and CFD simulations. Table 1 presents an overview of the wind-tunnel experiments and CFD simulations of convective heat transfer performed on wall-mounted rectangular prisms. It can be observed that:

- Most of the available high-resolution wind-tunnel data of CHTC are based on measurements at relatively low Reynolds numbers (10^3–10^4) [22–25], which limits the applicability of the available data for building applications.
- CFD simulations have been used to investigate CHTC at realistic Reynolds numbers for building applications (Re ~ 10^6–10^7) as, unlike wind-tunnel testing, CFD does not suffer from potentially incompatible similarity requirements because simulations can be conducted at full scale [26,27]. The impact of the reference wind speed (or Re), building geometry and urban surroundings have been investigated. However, not all studies have resolved the flow in the thin viscous sublayer at the building surfaces that constitutes the largest resistance to surface convective heat transfer, as this requires very small cells in the near wall region (typically a few ten or hundreds of micrometer).
- The combined effects of different parameters on CHTC have been taken into account in only a few studies. Natarajan and Chyu [23], Emmel et al. [8], and Blocken et al. [9] investigated the combined effect of Re and wind direction and presented CHTC expressions as a function of Re for different approaching wind directions. Montazeri et al. [4] and Montazeri and Blocken [6] investigated the combined impact of Re and building dimensions. The results of the latter studies led to new generalized expressions for the surface-averaged CHTC for different building surfaces as a function of reference wind speed, and height and width of the windward facade.

Earlier studies have shown that the use of existing CHTC expressions may lead to incorrect results in building energy simulations (BES). For example, using different expressions has revealed deviations of more than 30% in the yearly cooling energy demand of a simple low-rise building [20]. For high-rise buildings, the deviations could go up to 42% [28]. The above-mentioned shortcomings of the existing CHTC expressions and these of their underlying primary data sources indicate the need for more research efforts in terms of wind-tunnel testing, CFD simulations and the establishment of new and more generally applicable CHTC expressions. This paper is intended to provide a further step in that direction.

In this paper, new high-resolution CFD simulations of wind flow and forced convective heat transfer are performed, and a new generalized CHTC expression is presented that yields the surface-averaged forced CHTC for the windward facade of buildings as a function of four parameters: wind speed, building height, building width and wind direction.

It should be noted that in BES (building energy simulation) and BE-HAM (building envelope heat, air and moisture transfer) tools, generally three categories of CHTC models (expressions) are implemented with respect to surface orientation regarding the wind direction, i.e., CHTC models for windward facades, leeward facades and roofs. The focus in the present paper is on windward building facades because previous experimental and numerical studies indicated that the highest surface-averaged CHTC for wall-mounted rectangular prisms is obtained for the windward surface (e.g. Ref. [37]). The lowest CHTC is found for the leeward surfaces where the CHTC is rather insensitive to the wind direction and the building geometry [6,23]. In addition, in BE-HAM programs, the windward facade is the one that is wetted by wind-driven rain and for which knowledge of CHTC and of the related CMTC (convective moisture transfer coefficients) is of particular importance [38–40].

The results of this study will bring a better understanding of the interaction between the CHTC and its influencing parameters wind speed, building height, building width and wind direction at the windward facades of buildings. In addition, this study will lead to a new generalized CHTC expression for windward building facades, intending to support more accurate BES and BE-HAM simulations.

The outline of the paper is as follows. The wind-tunnel experiments of surface temperature at the surfaces of a wall-mounted cube by Meinders et al. [24] and the validation study are briefly presented in Section 2. Section 3 describes the computational settings and

Table 1
Overview of studies on forced convective heat transfer at wall-mounted rectangular prisms based on wind tunnel or CFD.

Authors (year)	Ref.	Re	Geometry	Flow direction (interval) (°)	Methodology	Heat transfer mechanism	Parameters
Meroney (1978)	[10]	3×10^4	S/RecPri[1]	0–90 (22.5)	WT	FC	θ
Chyu & Natarajan (1991)	[22]	$3.1 \times 10^3 - 1.1 \times 10^4$	S/Cube	0	WT	FC	Re
Natarajan & Chyu (1994)	[23]	$3.1 \times 10^4 - 1.0 \times 10^5$	S/Cube	0–45 (5)	WT	FC	Re, θ
Meinders et al. (1998)	[29]	$7.9 \times 10^2 - 5.1 \times 10^3$	A/Cube	0	WT	FC	Re
Meinders et al. (1999)	[24]	$2.7 \times 10^3 - 4.9 \times 10^3$	S/Cube	0	WT	FC	Re
Meinders & Hanjalić (1999)	[30]	$2.7 \times 10^3 - 4.9 \times 10^3$	M/Cube	0	WT	FC	Re
Nakamura et al. (2001)	[25]	$4.2 \times 10^3 - 3.3 \times 10^4$	S/Cube	0	WT	FC	Re
Meinders & Hanjalic (2002)	[31]	3.9×10^3	A/Cube	0	WT	FC	Arrang
Nakamura et al. (2003)	[32]	$4.2 \times 10^3 - 3.3 \times 10^4$	S/Cube	45	WT	FC	Re, θ^2
Yaghoubi & Velayati (2005)	[33]	$4.2 \times 10^3 - 1 \times 10^5$	A/Cube	0	CFD, no VS	FC	Re
Wang & Chiou (2006)	[34]	$0.8 \times 10^3 - 5.0 \times 10^3$	S/RecPri	0	WT	FC	Re
Emmel et al. (2007)	[8]	$1.8 \times 10^5 - 2.8 \times 10^6$	S/RecPri	0–90 (45)	CFD, no VS	FC	Re, θ^2
Blocken et al. (2009)	[9]	$0.7 \times 10^6 - 2.7 \times 10^6$	S/Cube	0–90 (11.25)	CFD, VS	FC	Re, θ^2
Defraeye et al. (2010)	[35]	$3.5 \times 10^4 - 3.5 \times 10^6$	S/Cube	0	CFD, VS	FC	Re
Allegrini et al. (2012)	[1]	$8.51 \times 10^5 - 3.4 \times 10^7$	S/RecPri[3]	0	CFD, no VS	FC, NC	Re
Liu et al. (2015)	[36]	$5.51 \times 10^5 - 1.4 \times 10^7$	S/Cube	0	CFD, VS	FC, NC	Re, λ_p
Montazeri et al. (2015)	[4]	$0.7 \times 10^6 - 2.8 \times 10^7$	S/RecPri[4]	0	CFD, VS	FC	Re, W, H
Montazeri & Blocken (2017)	[6]	$0.7 \times 10^6 - 8.5 \times 10^6$	S/RecPri[5]	0	CFD, VS	FC	Re, W, H

S = single (isolated) obstacle, RecPri = rectangular prism, A = arrays of obstacles, M = matrix of obstacles, WT = wind tunnel measurement, CFD = computational fluid dynamics, VS: viscous sublayer is resolved, no VS: viscous sublayer is not resolved, FC = forced convection, NC = natural convection, θ = flow direction, Re = Reynolds number, Arrang = arrangement of obstacles, λ_p = plan area density, W = width of obstacle, H = height of obstacle.
[1] Measurements were performed for three geometries with the same height (H = 0.153 m).
[2] For each of the flow directions, CHTC expressions are provided as a function of Re.
[3] 4 different geometries are considered.
[4] 22 different geometries are considered. Width (W) and height (H) of the windward surface vary from 10 m to 80 m.
[5] 81 different geometries are considered. W and H vary from 5 m to 80 m.

parameters for CFD simulations. Section 4 presents the CFD results, the new CHTC expression and in-sample and out-of-sample evaluations of the new expression. A discussion on the limitations of the study and the main conclusions are presented in Sections 5 and 6.

2. CFD validation study

In this study, the wind-tunnel measurements by Meinders et al. [24,37] are used for the CFD validation. Because this validation study has been published as a separate paper [4], it is only briefly presented here.

Meinders et al. [24,37] determined the exterior convective heat transfer at the surfaces of a cube (H_c = 0.015 m) in developing turbulent channel flow. The channel had dimensions width × height = 0.6 × 0.05 m^2. Experiments were conducted for several Reynolds numbers (based on H_c) ranging from 2000 to 5000. Laser-Doppler anemometry was used to measure the approach-flow turbulent boundary layer mean velocity and turbulent kinetic energy, while the external surface temperature distribution of the cube surface was measured with infrared thermography.

For the validation study, Re = 4440 is considered. The 3D steady RANS equations are solved with the commercial CFD code Ansys/Fluent 12.1 [41]. The realizable k-ε model (Rk-ε) [42] is used in combination with the low-Re number Wolfshtein model [43] for closure. The SIMPLE algorithm is used for pressure-velocity coupling, pressure interpolation is second order, and second-order discretization schemes are used for both the convection terms and the viscous terms of the governing equations. All other settings and parameters are reported in the previous validation study [4].

Fig. 1 compares the wind-tunnel results and CFD results of surface temperature along lines in a vertical and horizontal midplane on the windward surface of the cube. The general agreement is good. In this case, the average deviation along the vertical and horizontal lines is about 1.7 and 2.4%, respectively. This is also in line with the LES results by Iousef et al. [44] and Hu et al. [45]. Nevertheless, some overestimations can be clearly seen close to the ground. The main reason for these overestimations is not clear. But it could be due to additional heat loss through the base wall in the experiment, which is not taken into account in the simulations [4,44]. Another reason could be related to an incorrect prediction of the size and shape of the standing vortex due to the upstream longitudinal gradients in the approach-flow profiles [46,47]. Less good agreements are found for the other surfaces (not shown in Fig. 1) that are attributed to the well-documented inaccurate flow field prediction by steady RANS downstream of the windward facade [26,27,44,48–50]. Given the good agreements between CFD and wind-tunnel experiments for the windward surface and the fact that the focus of this study is on the windward facade of buildings, the computational parameters, and settings of the validation study are also used for the CFD simulations for the full-scale buildings.

3. CFD simulations for full-scale buildings

3.1. List of cases

The simulations for establishment of the expression are performed for 64 different building geometries, 8 wind directions, and 4 reference wind speeds. In addition, simulations are performed for out-of-sample evaluation of the expressions for additional building geometries, wind directions, and reference wind speeds. In total 625 simulations are performed. The simulations can be classified into three groups (Table 2):

- Group 1: simulations to obtain a correlation between the surface-averaged CHTC on the windward facade and the reference wind speed (U_{10}). Simulations are performed for 13 different building geometries (10 m ≤ H ≤ 40 m and 10 m ≤ W ≤ 80 m), 4 wind directions (θ = 0°, 22.5°, 45°, 67.5°), and 4 reference wind speeds U_{10} = 1, 2, 3, and 4 m/s.
- Group 2: simulations to obtain the new generalized expression for surface-averaged CHTC as a function of reference wind speed (U_{10}), building dimensions (H and W) and wind direction (θ). Simulations are performed for 64 building geometries (10 m ≤ H and W ≤ 80 m), 8 reference wind directions (0° ≤ θ ≤ 78.75° with 11.25° intervals) and for U_{10} = 1 m/s.
- Group 3: simulations for the out-of-sample evaluation of the new expression. Simulations are performed for 2 additional building

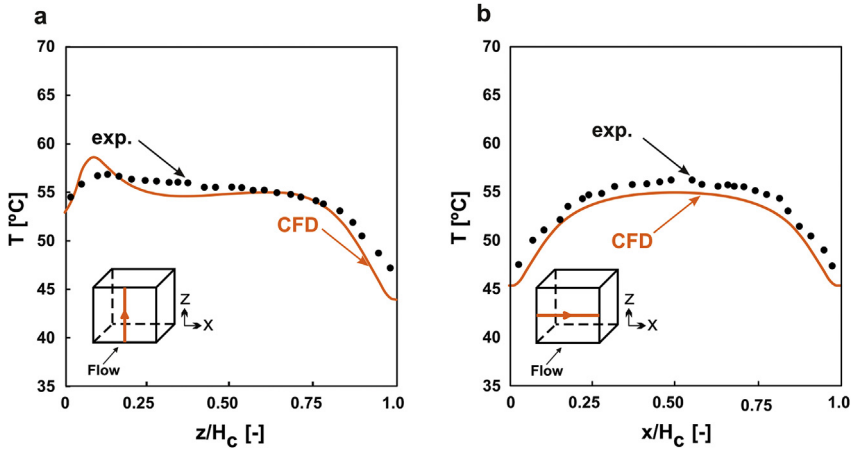

Fig. 1. Comparison of numerically simulated and measured surface temperature along (a) a vertical and (b) a horizontal line on the windward surface.

geometries with dimensions within the range of original data (Group 2) and 4 building geometries beyond the range of the original data. In this case, 6 reference wind directions (θ = 0°, 17°, 28°, 39°, 51° and 62°) and 4 reference wind speeds (U_{10} = 1, 1.5, 2.5 and 3.5 m/s) are considered.

3.2. Computational domain and gird

The dimensions of the computational domain are chosen based on the best practice guidelines by Tominaga et al. [51] and Franke et al. [52]. In this case, the upstream and downstream domain lengths are 5H and 15H, respectively. The height of the domain is 6H. As shown in the literature, a properly sized computational domain is of high importance for accurate CFD simulations of various applications, e.g. Refs. [53,54]. A high-resolution hybrid grid with prismatic and hexahedral cells is generated using the surface-grid extrusion technique [55], resulting in 1,911,316 cells (Fig. 2). The distance from the center point of the wall-adjacent cell to the wall, y_p, is about 400 μm, which leads to a maximum y* value below 5 for all building geometries, reference wind speeds, and wind directions.

3.3. Computational settings and parameters

At the inlet of the domain, neutral atmospheric boundary layer inflow profiles of mean wind speed U (m/s), turbulent kinetic energy k (m^2/s^2) and turbulence dissipation rate ε (m^2/s^3) are imposed:

$$U(z) = \frac{u^*_{ABL}}{\kappa} \ln\left(\frac{z + z_0}{z_0}\right) \quad (1)$$

$$k(z) = 1.5(I_U(z)U(z))^2 \quad (2)$$

$$\varepsilon(z) = \frac{u^{*3}}{\kappa(z+z_0)} \quad (3)$$

The buildings are assumed to be situated on a large grass-covered terrain with an aerodynamic roughness length z_0 = 0.03 m [56]. The reference wind speed at 10 m height, U_{10}, ranges from 1 to 4 m/s, resulting in building Re (based on the building height H) ranging from 0.7×10^6 to 8.5×10^6. Note that the use of the relatively low reference wind speeds is to avoid a prohibitively high total number of computational cells and the need for excessive computational resources, because the thickness of the viscous sublayer at the building surfaces decreases with increasing Re. For all simulations, the longitudinal turbulence intensity I_u, that is imposed at the inlet ranges from 20% at ground level with exponential decay to 5% at gradient height. The turbulent kinetic energy k is calculated from U and I_u using Eq. (2) and assuming that the standard deviations of the turbulent fluctuations in the three directions are similar ($\sigma_u = \sigma_v = \sigma_w$). The building and ground surfaces are considered smooth no-slip walls. Zero static pressure is applied at the outlet plane. Symmetry conditions (zero normal velocity and zero gradients) are applied at the top and lateral sides of the domain. The thermal boundary conditions are a uniform inlet air temperature of 10 °C and a fixed surface temperature of 30 °C for the building surfaces. In this study, only forced convection is considered and buoyancy effect is assumed negligible. Therefore, the CHTC is independent of the given temperature difference between the building surfaces and the air. It should be noted that there are different ways to define the CHTC using different definitions of the reference temperature. In this study, all CHTC values are determined based on the upstream (approach-flow) uniform temperature, at a position where it is unaffected by the presence of the building. The adiabatic boundary condition is used for the ground surface. Radiation and natural convection are not taken into account. The same solver settings as in the validation study (Section 2.2) are used. The 3D steady RANS equations are solved with the realizable k-ε turbulence model and the low-Re number Wolfshtein model. In the one-equation model of Wolfshtein, the turbulent viscosity, μ_t, and dissipation, ε, in the viscosity-affected near-wall region are computed from Eqs. (4) and (5):

$$\mu_t = \rho C_\mu l_\mu \sqrt{k} \quad (4)$$

$$\varepsilon = \frac{k^{3/2}}{l_\varepsilon} \quad (5)$$

where ρ is the density and k is the turbulent kinetic energy. The length scales l_μ and l_ε are given by Eqs. (6) and (7):

$$l_\mu = yC_l^*(1 - e^{-Re_y/A_\mu}) \quad (6)$$

$$l_\varepsilon = yC_l^*(1 - e^{-Re_y/A_\varepsilon}) \quad (7)$$

where y is the normal distance from the wall at the cell centers and the Re_y is the wall-based Re number $Re_y = \frac{\rho y\sqrt{k}}{\mu}$. The constants in Eqs. (6) and (7) are taken as $C_l^* = \kappa C_\mu^{-3/4}$, A_μ = 70 and $A_\varepsilon = 2C_l^*$.

4. Results

4.1. Relationship between CHTC and reference wind speed

The CFD simulations from Group 1 (Table 2) are used to obtain the relationship between the forced surface-averaged CHTC ($CHTC_{avg}$) and the reference wind speed U_{10}. Fig. 3 shows the results of the CFD simulations for the windward facade for θ = 0° and for different building geometries: (i) buildings with H = 10 m and W ranging from 10 to 80 m (Fig. 3a), (ii) buildings with W = 10 m and H ranging from 10 to 30 m

Table 2
Geometry of buildings and values of reference wind speed and wind direction.

Objective	Building geometry	No. of geometries	No. of simulations	Height (m)	Width (m)	Depth (m)	U_{10} (m/s)	θ (°)
GROUP 1: Obtain CHTC-U_{10} (Re) correlations	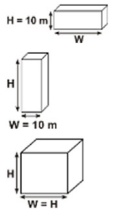	8	32	10	10, 20, 30, 40, 50, 60, 70, 80	20	1, 2, 3, 4	0
		1	12	10	40	20	1, 2, 3, 4	22.5, 45, 67.5
		3	12	10, 20, 30	10	20	1, 2, 3, 4	0
		1	12	40	10	20	1, 2, 3, 4	22.5, 45, 67.5
		3	12	10, 20, 30	W = H	20	1, 2, 3, 4	0
		1	12	10	W = H	20	1, 2, 3, 4	22.5, 45, 67.5
GROUP 2: Obtain CHTC- U_{10}, W, H and θ correlation	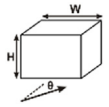	8	64	10	10, 20, 30, 40, 50, 60, 70, 80	20	1	0, 11.25, 22.5, 33.75, 45, 56.25, 67.5, 78.75
		8	64	20	10, 20, 30, 40, 50, 60, 70, 80	20	1	0, 11.25, 22.5, 33.75, 45, 56.25, 67.5, 78.75
		8	64	30	10, 20, 30, 40, 50, 60, 70, 80	20	1	0, 11.25, 22.5, 33.75, 45, 56.25, 67.5, 78.75
		8	64	40	10, 20, 30, 40, 50, 60, 70, 80	20	1	0, 11.25, 22.5, 33.75, 45, 56.25, 67.5, 78.75
		8	64	50	10, 20, 30, 40, 50, 60, 70, 80	20	1	0, 11.25, 22.5, 33.75, 45, 56.25, 67.5, 78.75
		8	64	60	10, 20, 30, 40, 50, 60, 70, 80	20	1	0, 11.25, 22.5, 33.75, 45, 56.25, 67.5, 78.75
		8	64	70	10, 20, 30, 40, 50, 60, 70, 80	20	1	0, 11.25, 22.5, 33.75, 45, 56.25, 67.5, 78.75
		8	64	80	10, 20, 30, 40, 50, 60, 70, 80	20	1	0, 11.25, 22.5, 33.75, 45, 56.25, 67.5, 78.75
GROUP 3: Out-of-sample fit evaluation	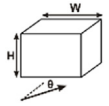	1	20	35	25	20	1.5, 2.5, 3.5	17, 28, 39, 51, 62
		1	20	15	65	20	1.5, 2.5, 3.5	17, 28, 39, 51, 62
		1	1	20	90	20	1	0
		1	1	60	90	20	1	0
		1	1	30	100	20	1	0
		1	1	40	100	20	1	0

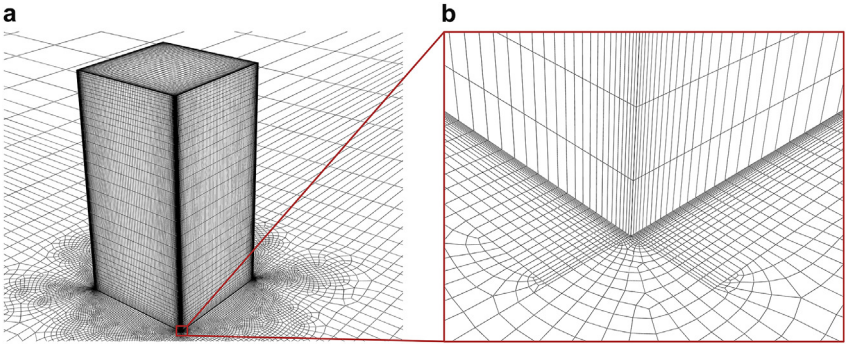

Fig. 2. High-resolution grid at building surfaces and part of the ground surface for building H = 40 m and W = 20 m (total number of cells: 1,911,316).

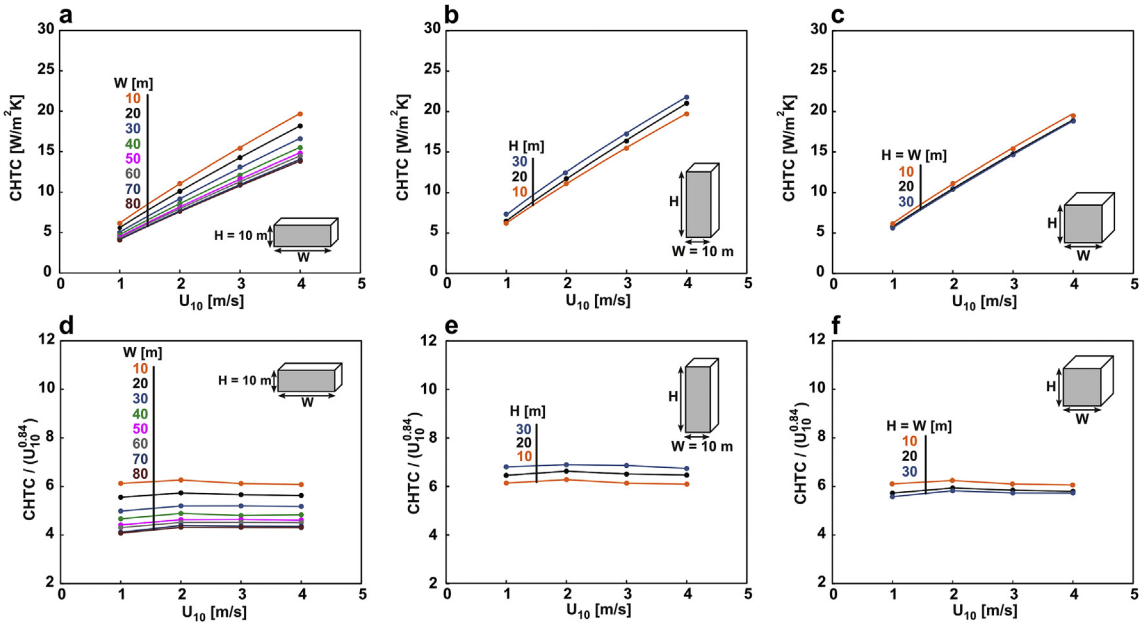

Fig. 3. Surface-averaged CHTC on the windward facade as a function of U_{10} for buildings with (a) H ≤ W, (b) H ≥ W and (c) H = W. (d,e,f) Same for ratio $CHTC_{avg}/(U_{10}^{0.84})$.

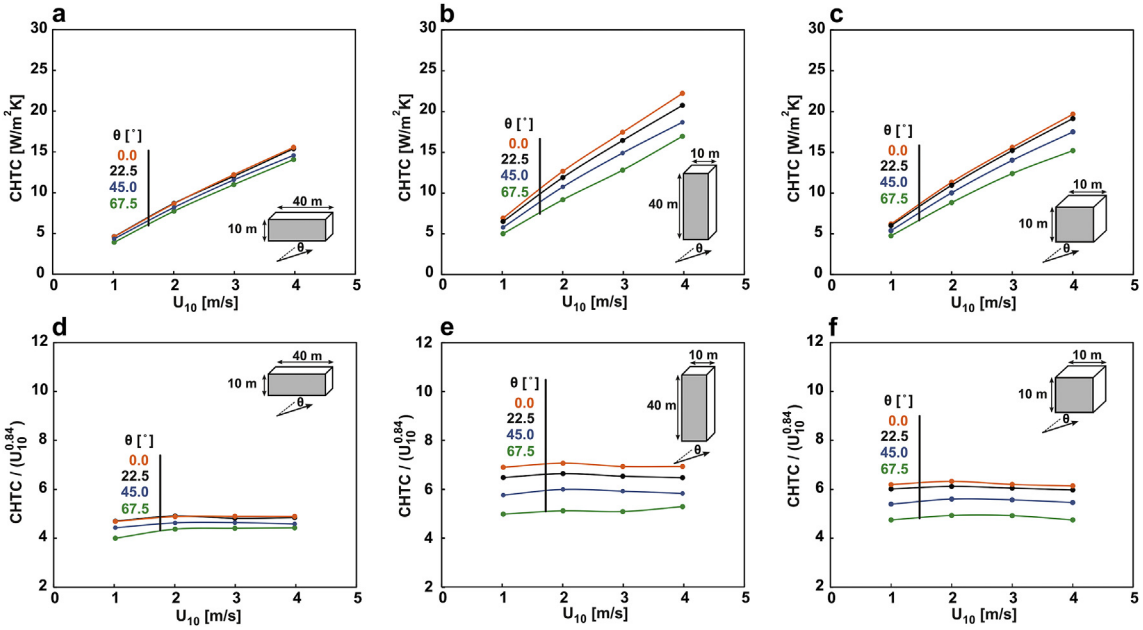

Fig. 4. Surface-averaged CHTC on the windward facade of building with (a) H = 10 m and W = 40 m, (b) H = 40 m, W = 10, and (c) H = 10 m, W = 10 m as a function of U_{10} for different reference wind directions. (d,e,f) Same for ratio $CHTC_{avg}/(U_{10}^{0.84})$.

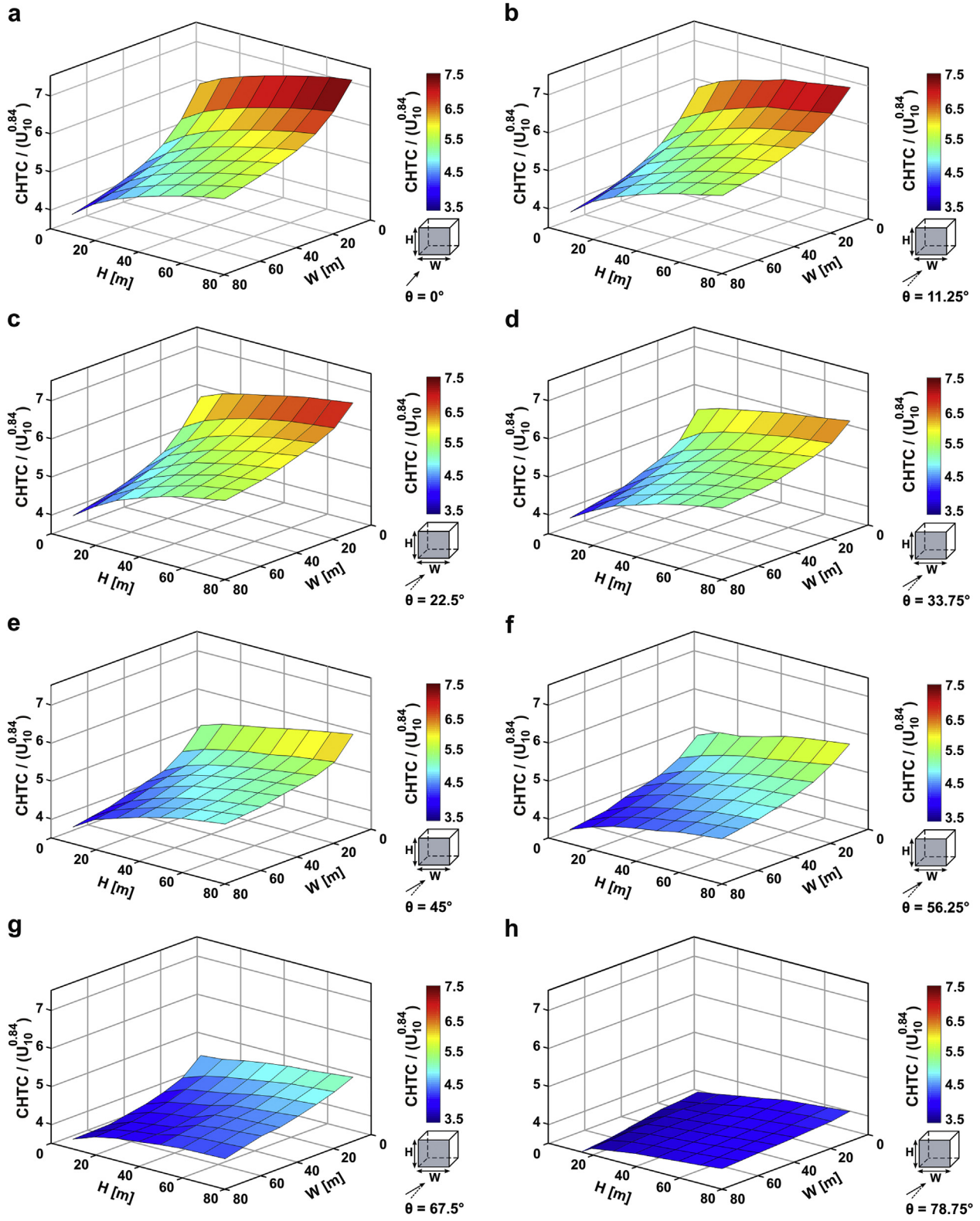

Fig. 5. (a–h) Surface-averaged ratio ($CHTC/U_{10}^{0.84}$) on the windward facade as a function of H and W for wind directions θ = 0°, 11.25°, 22.5°, 33.75°, 45°, 56.25°, 67.5°, 78.75°.

(Fig. 3b), and buildings with W = H ranging from 10 to 30 m (Fig. 3c). As pointed out by Montazeri and Blocken [6], based on fitting with power-law functions, the fit with power-law exponent 0.84 yields the best performance for all building geometries (R^2 = 0.9829 to 0.9994). This is also indicated in Fig. 3d–f, where the parameter $CHTC_{avg}/U_{10}^{0.84}$ is plotted versus U_{10}. It appears that for a given building geometry, the ratio $CHTC_{avg}/U_{10}^{0.84}$ is independent of U_{10} for wind directions perpendicular to the windward facade. Fig. 4a–c indicates profiles of the $CHTC_{avg}$ at the windward facade of the buildings with H = 10 m and W = 40 m (Fig. 4a), H = 40 m and W = 10 m (Fig. 4b) and H = W =

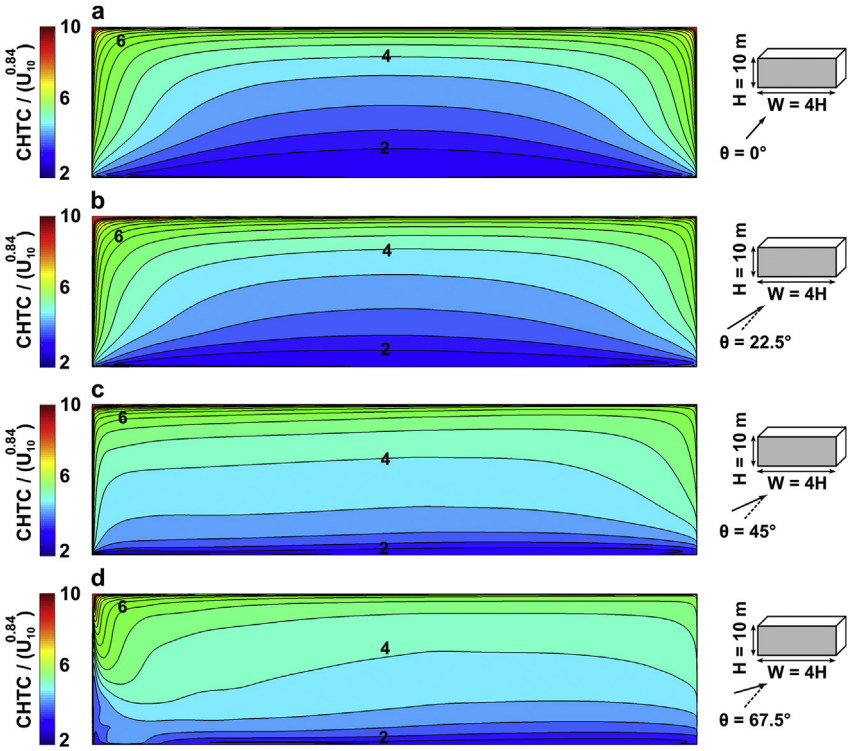

Fig. 6. Distribution of ratio CHTC/($U_{10}^{0.84}$) across the windward facade for buildings with H = 10 m and W = 4H = 40 m for different wind directions: (a) θ = 0°, (b) θ = 22.5°, (c) θ = 45° and (d) θ = 67.5° (D = 20 m for all cases).

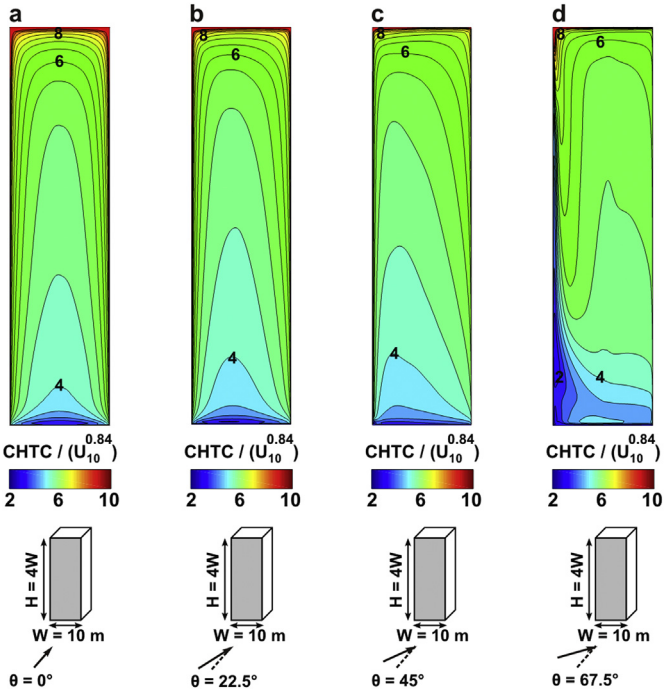

Fig. 7. Distribution of ratio CHTC/($U_{10}^{0.84}$) across the windward facade for buildings with W = 10 m and H = 4W = 40 m for different wind directions: (a) θ = 0°, (b) θ = 22.5°, (c) θ = 45° and (d) θ = 67.5° (D = 20 m for all cases).

10 m (Fig. 4c) as a function of U_{10} for different reference wind directions. The ratio $CHTC_{avg}/U_{10}^{0.84}$ for these three geometries is presented in Fig. 4d–f. It can be seen that for a given building geometry, the ratio $CHTC_{avg}/U_{10}^{0.84}$ is nearly independent of U_{10} for these different reference wind directions. This indicates that the establishment of the relationship between $CHTC_{avg}$, building height, and width and reference wind direction can be performed for only a single value of U_{10}. Therefore, this approach is adopted in the next subsection. Afterwards, out-of-sample evaluations will be performed to validate this approach.

4.2. New CHTC expression

To establish the relationship between the surface-averaged CHTC ($CHTC_{avg}$), building height (H), building width (W) and wind direction (θ), the simulations from Group 2 (Table 2) are used (512 simulations). As the ratio $CHTC_{avg}/U_{10}^{0.84}$ is independent of U_{10} for different values of H, W and θ, all simulations are performed at U_{10} = 1 m/s (see Section 4.1 and Figs. 3 and 4).

Fig. 5 displays the ratio $CHTC_{avg}/U_{10}^{0.84}$ for the windward facade as a function of W and H for different wind directions. The following observations can be made:

- For a given wind direction, by increasing the building height (H), the ratio $CHTC_{avg}/U_{10}^{0.84}$ increases. For example, for buildings with W = 40 m, as H increases from 10 m to 80 m, the ratio $CHTC_{avg}/U_{10}^{0.84}$ increases by about 26%, 25%, 19% and 16% for θ = 0°, 22.5°, 45° and 67.5°, respectively. This increase is related to increase of wind speed with height in the atmospheric boundary layer, which in turn increases the local wind speed values at the lateral and top edges of the windward facades for higher values of H.
- For a given wind direction, increasing the building width (W), however, has the opposite impact on the ratio $CHTC_{avg}/U_{10}^{0.84}$. For buildings with H = 40 m, for example, as W increases from 10 m to 80 m, the ratio $CHTC_{avg}/U_{10}^{0.84}$ decreases by about 25%, 19%, 17% and 16% for θ = 0°, 22.5°, 45° and 67.5°, respectively. Note that increasing the width of the buildings results in a more pronounced wind-blocking effect upstream of the building, which reduces the local wind speeds near the windward facade. This also increases the time that the air is in contact with the facade, which reduces the temperature difference between the air and the surface especially for the top and edges of the facade. These phenomena lead to a

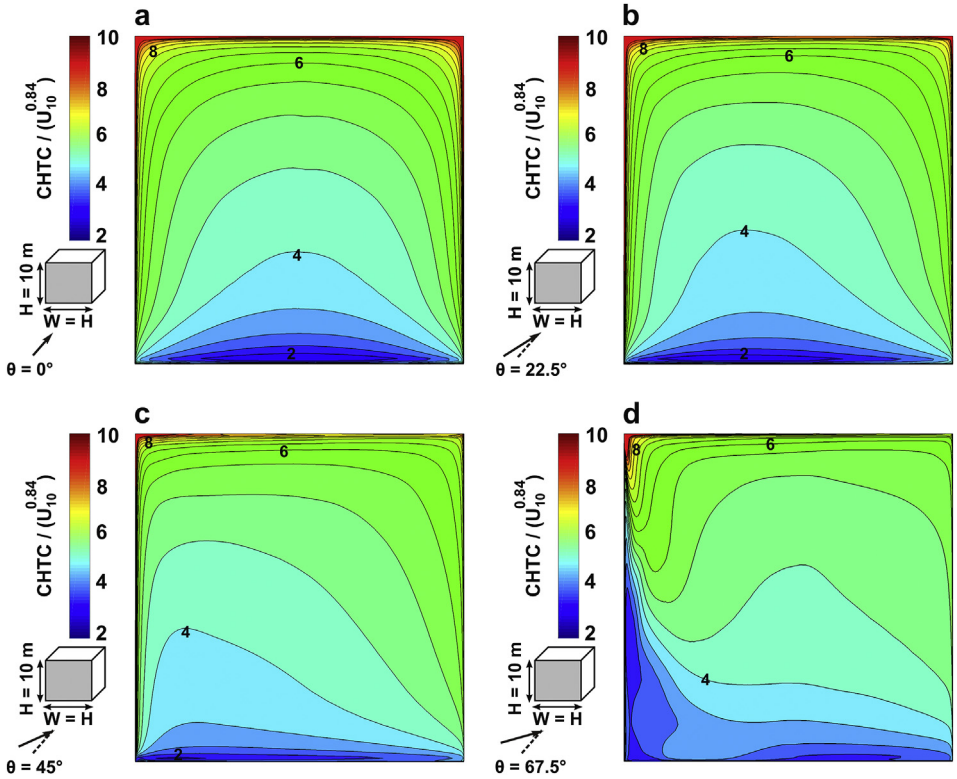

Fig. 8. Distribution of ratio CHTC/($U_{10}^{0.84}$) across the windward facade for buildings with H = W = 10 m for different wind directions: (a) θ = 0°, (b) θ = 22.5°, (c) θ = 45° and (d) θ = 67.5° (D = 20 m for all cases).

reduction in the local and surface-averaged CHTC/$U_{10}^{0.84}$.

- For a given building geometry (constant height and width of the windward facade), the ratio $CHTC_{avg}/U_{10}^{0.84}$ reduces as the reference wind direction increases. This is because the local and surface-averaged CHTC at the surfaces of a bluff body are highly dependent on the immediate flow structure around the obstacle [4,9,57,58] that substantially varies by changing the wind direction [59]. Fig. 6 shows the ratio CHTC/$U_{10}^{0.84}$ across the windward facade of the building with H = 10 m and W = 4H = 40 m for different reference wind directions. Figs. 7 and 8 show the same results for the building with H = 4W = 40 m and W = 10 m, and H = W = 10 m, respectively. It can be seen that at θ = 0°, the maximum CHTC/$U_{10}^{0.84}$ value occurs at the top and lateral edges where the wind speed is relatively high. A relatively uniform CHTC/$U_{10}^{0.84}$ distribution is observed over the central area of the windward facade, which corresponds to the uniform high-pressure and low-velocity zones in this part of the facade. The minimum local CHTC/$U_{10}^{0.84}$ is observed in the lower part of the facade, near the region where the horseshoe vortex occurs. This is due to the rotational behavior of the vortex, which increases the residence time of the air in this region leading to an increase in the local air temperature and a reduction of the local value of CHTC/$U_{10}^{0.84}$ [4]. By increasing the wind direction, for all building geometries, the CHTC/$U_{10}^{0.84}$ distribution becomes asymmetric, where the maximum CHTC across the windward facade occurs near the upper most upstream corner of the windward facade. For the cases with θ ≤ 45°, the lowest values are observed in the lower part of the facade. For θ = 67.5°, however, the minimum CHTC/$U_{10}^{0.84}$values occur close to the upstream edge of the facade because of the dominance of flow separation and recirculation at this flow direction. This is in line with the wind-tunnel measurements of Natarajan and Chyu [23], though in those measurements the boundary layer thickness was relatively thin, i.e., about 1/4 to 1/3 of the cube height.

In this study, a polynomial is used to fit the CFD data in four dimensions (CHTC/U_{10}, H, W and θ) and to yield the CHTC expression as a function of the four parameters (U_{10}, H, W, θ). This polynomial can subsequently be used to obtain values for the CHTC by interpolation or by extrapolation. However, as pointed out by Montazeri and Blocken [6], the use of polynomials beyond the original data should be treated with caution because of the rather large extrapolation errors that can occur with polynomials. In the present study, the following steps are taken to improve the performance of the polynomial beyond the original data:

- For a given value of wind direction and building width, the CFD results for different building heights, Group 2 in Table 2 (10 m ≤ H ≤ 80 m), are used to generate additional data for 90 m ≤ H ≤ 150 m using two-dimensional fitting. A sensitivity analysis shows that the power-law functions yield the best performance to describe the correlation between $CHTC_{avg}/U_{10}^{0.84}$ and H. For example, for θ = 0° and W = 10 m, the fit with power-law exponent 0.085 yields the best performance. Therefore, the power-law function $CHTC_{avg}/U_{10}^{0.84} = 5.05H^{0.085}$ is implemented to obtain data beyond the original data for buildings with H = 90, 100, 110, 120, 130, 140 and 150 m.
- The abovementioned procedure is used to obtain additional data for different building heights (90 m ≤ H ≤ 150 m) for all wind directions and building widths mentioned in Group 2 of Table 2.
- For a given value of wind direction and building height, the CFD results for different building widths (10 m ≤ W ≤ 80 m) are used to generate additional data for 90 m ≤ W ≤ 150 m using two-dimensional fitting. In this case, the logarithmic functions are found to be superior to fit the CFD data.
- The abovementioned procedure is used to obtain additional data for different building widths (90 m ≤ W ≤ 150 m) for all wind directions and building heights mentioned in Group 2 of Table 2.

Table 3
Expression for forced surface-averaged CHTC on the windward facade as a function of reference wind speed U_{10}, building dimensions H and W and wind direction θ.

$$CHTC = U_{10}^{0.84}.(a_0 + a_1.W + a_2.W^2 + a_3.W^3 + a_4.W^4 + a_5.H + a_6.H^2 + a_7.H^3 + a_8.H^4 + a_9.\theta + a_{10}.\theta^2 + a_{11}.\theta^3 + a_{12}.\theta^4 + a_{13}.W.H + a_{14}.W.H^2 + a_{15}.W.H^3 + a_{16}.W.\theta + a_{17}.W.\theta^2 + a_{18}.W.\theta^3 + a_{19}.W^2.H + a_{20}.W^2.H^2 + a_{21}.W^2.H^3 + a_{22}.W^2.\theta + a_{23}.W^2.\theta^2 + a_{24}.W^2.\theta^3 + a_{25}.W^3.H + a_{26}.W^3.H^2 + a_{27}.W^3.H^3 + a_{28}.W^3.\theta + a_{29}.W^3.\theta^2 + a_{30}.W^3.\theta^3 + a_{31}.H.\theta + a_{32}.H.\theta^2 + a_{33}.H.\theta^3 + a_{34}.H^2.\theta + a_{35}.H^2.\theta^2 + a_{36}.H^2.\theta^3 + a_{37}.H^3.\theta + a_{38}.H^3.\theta^2 + a_{39}.H^3.\theta^3)$$

$a_0 = 6.584$	$a_1 = -8.761E-2$	$a_2 = 1.009E-3$	$a_3 = -5.668E-6$
$a_4 = 1.166E-8$	$a_5 = 3.769E-2$	$a_6 = -4.649E-4$	$a_7 = 3.214E-6$
$a_8 = -8.676E-9$	$a_9 = -5.991E-2$	$a_{10} = 1.506E-3$	$a_{11} = -1.305E-5$
$a_{12} = -1.865E-8$	$a_{13} = 3.968E-4$	$a_{14} = -3.683E-6$	$a_{15} = 1.281E-8$
$a_{16} = 1.593E-3$	$a_{17} = -3.984E-5$	$a_{18} = 3.559E-7$	$a_{19} = -3.737E-6$
$a_{20} = 3.657E-8$	$a_{21} = -1.296E-10$	$a_{22} = -1.390E-5$	$a_{23} = 3.473E-7$
$a_{24} = -3.092E-9$	$a_{25} = 1.224E-8$	$a_{26} = -1.235E-10$	$a_{27} = 4.433E-13$
$a_{28} = 4.544E-8$	$a_{29} = -1.133E-9$	$a_{30} = 1.002E-11$	$a_{31} = 6.239E-4$
$a_{32} = -2.694E-5$	$a_{33} = 2.006E-7$	$a_{34} = -6.178E-6$	$a_{35} = 2.428E-7$
$a_{36} = -1.828E-9$	$a_{37} = 2.047E-8$	$a_{38} = -8.424E-10$	$a_{39} = 6.410E-12$
$R^2 = 0.9919$			

- All original data obtained by CFD simulations (Group 2 in Table 2), and the additional data, obtained by the two-dimensional extrapolations (90 m ≤ H ≤ 150 m and 90 m ≤ W ≤ 150 m), are used to derive the new CHTC expression.

A fourth-order polynomial equation including cross-terms (i.e., terms involving the product of the independent variables) is used to express the ratio $CHTC_{avg}/U_{10}^{0.84}$ as a function of H, W and θ with a good approximation ($R^2 = 0.9919$). Table 3 presents the new CHTC expression as a function of U_{10}, H, W and θ. Using the coefficients with 2 decimal digits instead of 8 provides a deviation of about 0.21%. Using the coefficients with 3 decimal digits instead of 8 provides a deviation of only 0.010%. Therefore, only 3 decimal digits are retained in the table. The new expression can be easily implemented and used in numerical BES and BE-HAM programs.

4.3. In-sample and out-of-sample evaluation of new CHTC expression

In-sample and out-of-sample evaluations are performed to evaluate the accuracy of the new CHTC expression, presented in Table 3. The terms “in-sample” and “out-of-sample” evaluations refer to the assessment of the accuracy of the new CHTC expression within and beyond the range of the original CFD data, respectively. Fig. 9 illustrates the results of the in-sample evaluation in which the CHTC values obtained by the new expression are compared with the values directly obtained from the CFD simulations from Group 2 in Table 2. A very good agreement is observed with the high values of R^2 ranging from 0.9579 (θ = 78.75°) to 0.9981 (θ = 0°). Out-of-sample evaluations for combinations of the variables U_{10}, H, W and θ are performed by comparing with the CFD results (Group 3 in Table 2). Figs. 10 and 11 show that for all combinations the resulting values of surface-averaged CHTC are well predicted by the new expression. In this case, the maximum deviation is about 7%, which occurs for the building with H = 15 m and W = 65 m at θ = 62° for U = 2.5 m/s. The average deviation for all cases is about 4%. The related coefficient of determination is $R^2 = 0.9980$. Note that for the building geometries outside the range of those for which the CFD simulations were performed, the maximum deviation is 1.6% for the building with H = 60 m and W = 90 m (Fig. 11). The in-sample and out-of-sample evaluations provide confidence in the new expressions for an accurate prediction of the CHTC for different buildings.

4.4. New expression vs other CHTC models

Fig. 12 compares the $CHTC_{avg}$ values obtained by the new CHTC expression (presented in Table 3) and five commonly used CHTC expressions in BES tools with the values directly obtained from the CFD simulations. The results are presented for three different building geometries as a function of the reference wind speed and wind direction. The EmmelVertical [8], Nusselt-Jürges [21], McAdams [17], Mitchell [60] and TARP [61] expressions are considered. The calculations are based the implementations of these model in the BES tool EnergyPlus. It should be noted that EmmelVertcial is the only model in which wind direction is considered as a parameter. The TARP and Mitchell models implicitly consider building geometry [20], while Nusselt-Jürges and McAdams only include wind speed to describe the CHTC. It can be seen that the new expression (Table 3) provides a good agreement with the CFD results for different values of reference wind speed and wind direction. For the building with H = W = 10 m, for example, the deviation between the CFD results and the new expression results is about 0.8% for θ = 0° and U_{10} = 1 m/s. This is about 2.8%, 1.4% and 0.3% for θ = 22.5°, 45° and 67.5°, respectively. For the other expressions, however, the deviations can be very large. For the building with H = W = 10 m, the use of the Nusselt-Jürges expression, for example, leads to a deviation of about 48% for θ = 0° and U_{10} = 1 m/s. This deviation increases by increasing the wind direction and goes up to 93% for θ = 67.5°.

In addition, the $CHTC_{avg}$ values obtained by the new expression (Table 3) are compared with the values given by the existing generalized CHTC expression that contains the reference wind speed, the width and the height of the windward building facade as parameters [6]. The evaluation is performed for the 64 building geometries presented in Table 2 (Group 2, 10 m ≤ H ≤ 80 m and 10 m ≤ W ≤ 80 m) and for θ = 0°. The results show that the maximum and the average deviation between the CHTC values obtained by the two expressions are about 3.7% and 1.4%, respectively.

5. Discussion

In this study, a fourth-order polynomial equation including cross-terms (i.e., terms involving the product of the independent variables) is used to develop the new CHTC expression. The choice of the polynomial is based on a sensitivity analysis in which polynomials of different orders were evaluated. Six polynomials were considered: second, third

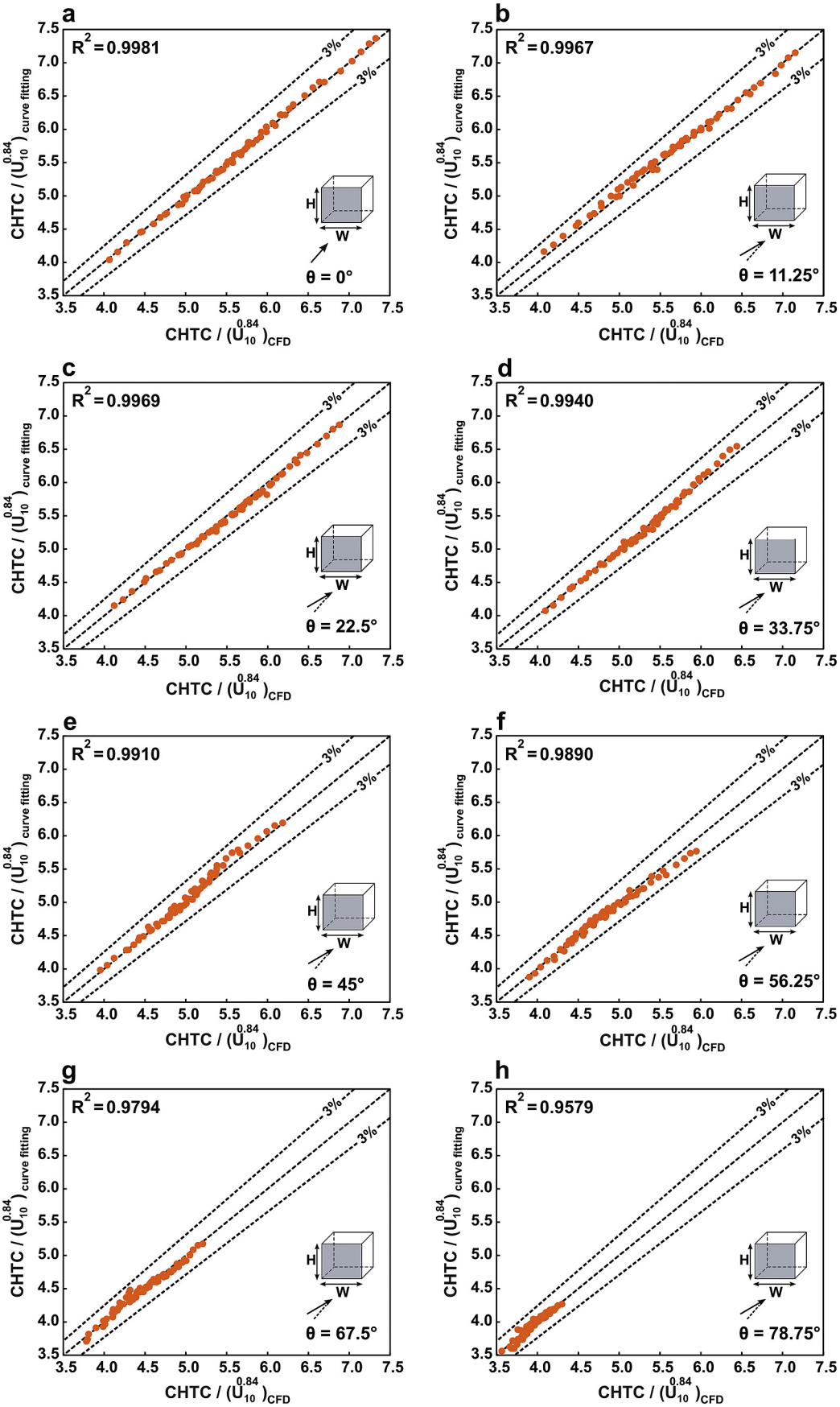

Fig. 9. (a–h) In-sample evaluation of the forced CHTC expression in Table 3: Fitted values of forced surface-averaged ratio ($CHTC/U_{10}^{0.84}$) on the windward facade versus values directly obtained by CFD as a function of H and W for wind directions θ = 0°, 11.25°, 22.5°, 33.75°, 45°, 56.25°, 67.5° and 78.75°.

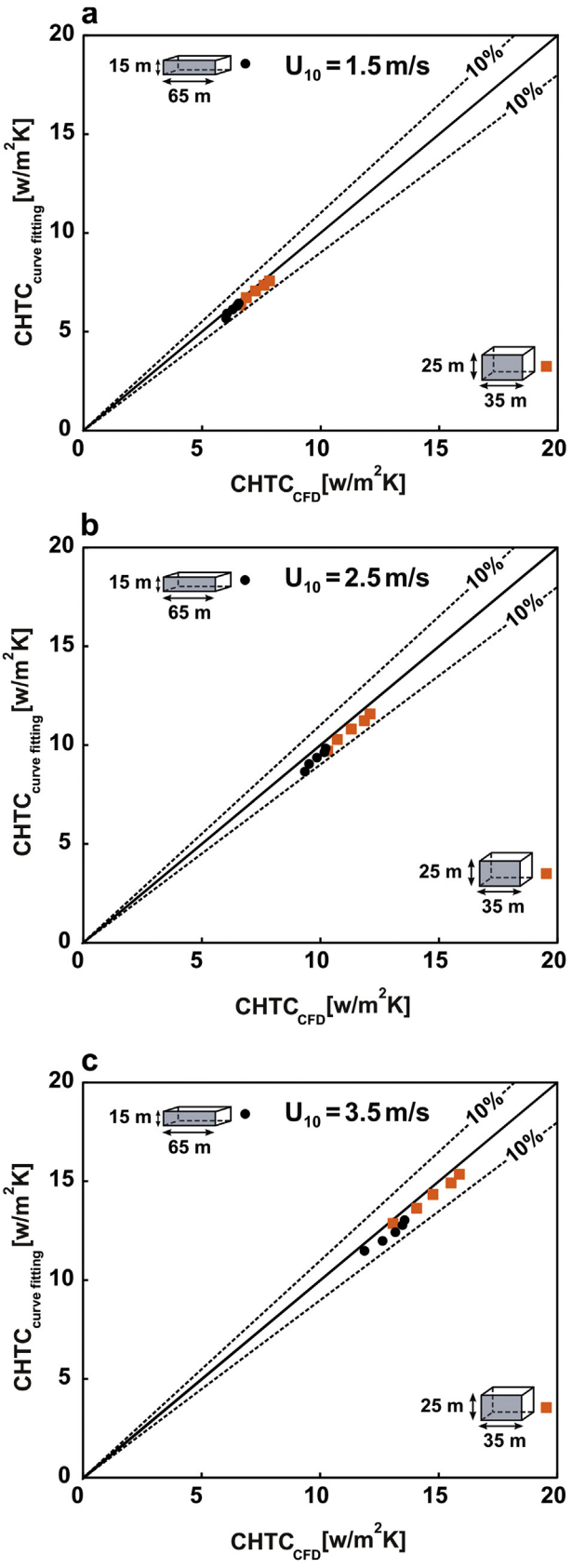

Fig. 10. Out-of-sample evaluation of the new CHTC expression in Table 3 for buildings with H = 25 m, W = 35 m and H = 15 m, W = 65 and five wind directions θ = 17°, 28°, 39°, 51° and 62° for U_{10} = (a) 1.5, (b) 2.5 and (c) 3.5 m/s.

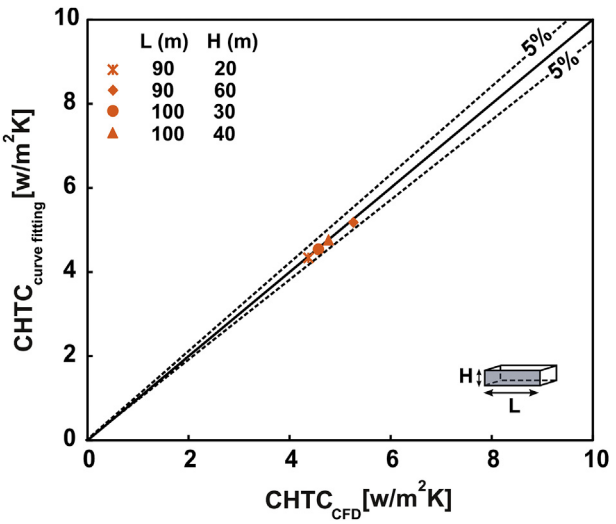

Fig. 11. Out-of-sample evaluation of the new CHTC expression in Table 3 for buildings with dimensions outside the range of the CFD data for θ = 0° and U_{10} = 1 m/s.

and fourth-order polynomials including and excluding cross-terms. The in-sample accuracy of the polynomials was evaluated by comparing the coefficients of determination (R^2). The results show that a fourth-order polynomial including cross-terms yields the best performance. The coefficients of determination for the second, third and fourth-order polynomials excluding cross-terms are 0.9171, 0.9270, and 0.9286, respectively. These are 0.9691, 0.9847 and 0.9919 for the polynomials including cross-terms, respectively. The good performance of four-order polynomials was also observed in a previous study [6].

The new expression contains wind speed, building height and width, and wind direction as separate parameters. The use of H and W as separate parameters, instead of non-dimensional parameters such as building aspect ratio (H/W), is because of the complex individual impact of H and W on the $CHTC_{avg}$ for different wind directions. For example, for buildings with H = W (H/W = 1) and at θ = 0°, increasing the building height and width from 10 m to 40 m yields a 10% reduction in the $CHTC_{avg}/(U_{10}{}^{0.84})$ on the windward facade. For higher values of H and W, however, the opposite trend is found. As H and W increase from 50 m to 80 m, the ratio $CHTC_{avg}/(U_{10}{}^{0.84})$ increases by 3%. Similar trends can also be seen for the other wind directions.

While this study has provided several new insights, and presented a new generalized CHTC expression for more accurate BES and BE-HAM simulations, it is also important to mention the limitations of this study:

- The validation study is performed for a wall-mounted cubic obstacle at a relatively low Reynolds number (Re = 4440). This is due to the lack of available high-resolution on-site or wind-tunnel data at realistic Reynolds numbers for building applications (Re ~ 10^6–10^7). It should be noted that the essential flow features such as impingement, the horse-shoe vortex, etc., and the level of flow complexity at both aforementioned regimes of Re are relatively similar. Therefore, it can reasonably be assumed that the given combination of computational parameters and settings that provided accurate simulation results in the validation study, will also provide accurate results for the full-scale buildings. Nevertheless, given the relatively low Reynolds number in the measurements, it is likely that the boundary layer over the windward surface of the cube is laminar, while the boundary layers over building surfaces are mostly turbulent. Future high-resolution experimental work is, therefore, required at sufficiently high Reynolds numbers to enable further validation of CFD simulations.
- No grid-sensitivity analysis is performed for the CFD simulations of

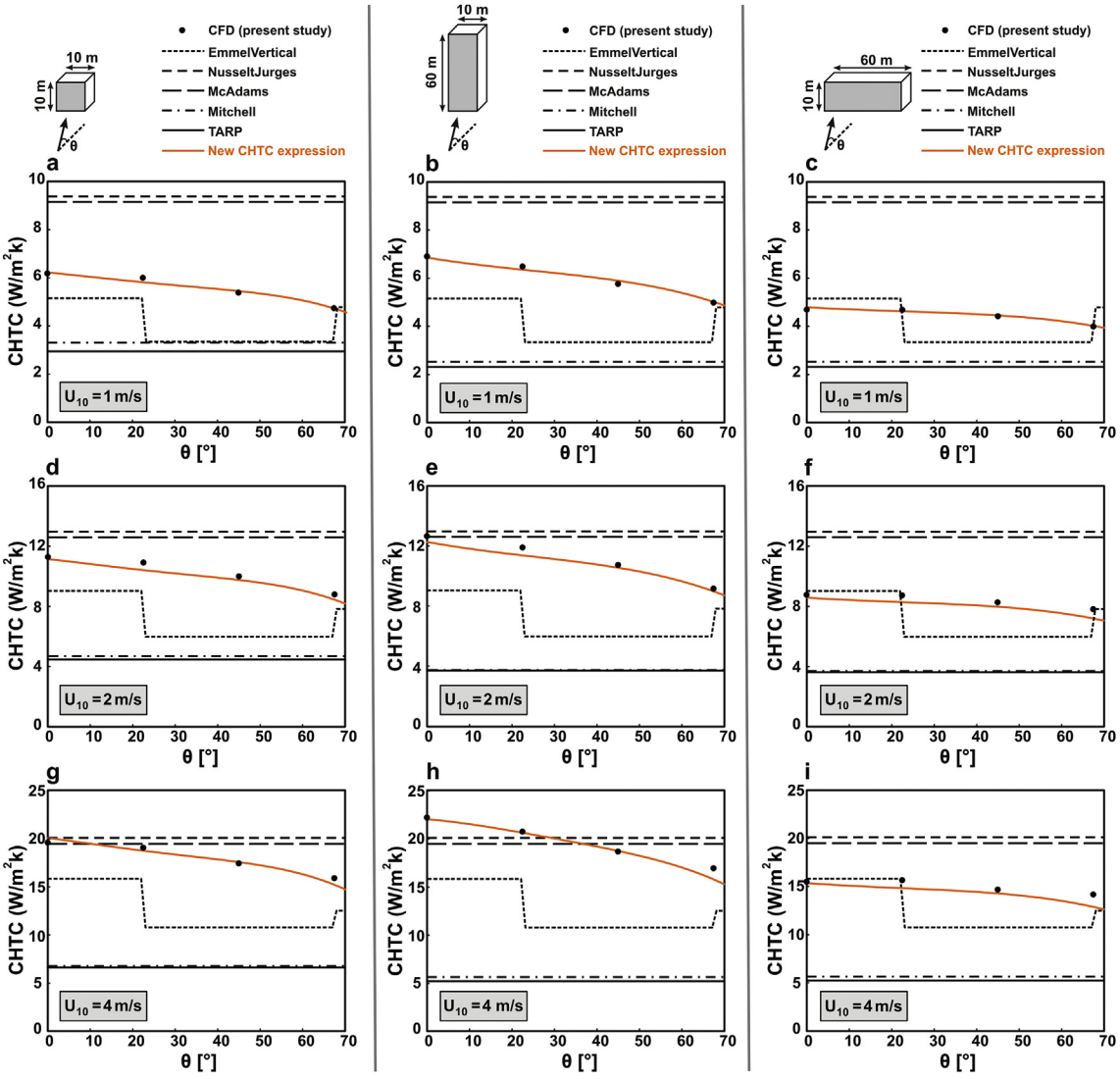

Fig. 12. Comparison between surface-averaged CHTC obtained by empirical expressions and new expression with CFD results as a function of wind direction for U_{10} = 1 m/s and for buildings with (a) H = 10 m and W = 10 m, (b) H = 60 m and W = 10 m and (c) H = 10 m and W = 60 m. Same for (d–f) U_{10} = 2 m/s and (g–i) U_{10} = 4 m/s.

the full-scale buildings. Nevertheless, special attention was paid to generating a high-resolution and high-quality computational grid with a minimum near-wall cell size of 400 μm ($y^* < 5$) to resolve the entire boundary layer, including the viscous sublayer and the buffer layer, which dominate the convective surface resistance. In addition, the grid was made according to best practice guidelines for grid generation [2,51,52,62,63].

- In this study, the simulations are performed for perfectly smooth building surfaces, which is generally an implicit assumption of low-Re number modeling when the geometry of roughness features is not modeled explicitly. Note that previous experimental studies have shown the importance of surface roughness (small-scale roughness) on the exterior CHTC [64,65]. In addition, other studies show the importance of large-scale roughness (building facades and roofs with protrusions or recessions) on local flow patterns [66–72]. Given the fact that building details, such as balconies, can lead to a strong change in the flow pattern around the building, this roughness scale can also considerably affect the CHTC distribution on building facades, and future CHTC studies should also focus on facades with this type of roughness.
- This study is limited to isolated buildings and is not valid for buildings surrounded by other buildings of similar height. Nevertheless, in many European cities, high-rise buildings are generally positioned among low-rise buildings, and not present in groups/clusters, as in more modern cities on the American continent. Therefore, they can, to some extent, be represented by an isolated building in this study. Note that considering the impact of building surroundings requires an extensive parametric study in which the individual and the combined effects of urban geometry parameters (e.g. frontal area density, plan area density and building height variations), wind speed, wind direction, and building geometry are investigated. Given the complexity of wind flow in urban areas, more accurate results should be pursued using transient simulations with LES. However, LES is computationally expensive especially for extensive parametric studies such as the present study in which numerous simulations are performed.
- In the present study, only forced convection is considered. Earlier studies have shown that buoyancy can be important in general, but especially in urban areas, where pavement and building facades are heated by the solar radiation, and wind speeds are significantly reduced because of wind sheltering [1]. The presence of the buoyancy driven flows can significantly change the structure of the flow around buildings and strengthen the intensity of the circulation within street canyons, resulting in significant changes in the CHTC

distribution on the building facades [73–75].

6. Summary and conclusions

In this study, the combined impacts of the reference wind speed (U_{10}), the height (H) and the width (W) of the windward building facade, and the reference wind direction (θ) on the surface-averaged forced CHTC ($CHTC_{avg}$) for the windward facade of buildings are investigated and a new generalized CHTC expression as a function of these parameters is presented. CFD simulations of wind flow and forced convective heat transfer are performed for 70 different building geometries, 8 wind directions ($0^\circ \le \theta \le 78.75^\circ$) and 4 reference wind speed values (1 m/s ≤ U_{10} ≤ 4 m/s). In total 625 simulations are performed. The 3D RANS equations with the realizable k-ε turbulence model and the low-Re number Wolfshtein model are used. The simulations are based on an extensive validation study with previously published wind-tunnel measurements. The following conclusions are made:

(a) The combined effects of U_{10}, H, W and θ on $CHTC_{avg}$
- For a given building geometry (constant height and width of the windward facade) and U_{10}, the surface-averaged $CHTC_{avg}$ reduces as the reference wind direction increases. This is because the local and surface-averaged CHTC at the surfaces of a bluff body are highly dependent on the immediate flow structure around the obstacle that substantially varies by changing the wind direction.
- For a given wind direction and U_{10}, by increasing the building height, the $CHTC_{avg}$ increases. Increasing the building width, however, has the opposite impact on the $CHTC_{avg}$.
- For a given U_{10} and for $\theta = 0^\circ$, the maximum CHTC value occurs at the top and lateral edges where the wind speed is relatively high. The minimum local CHTC is observed in the lower part of the facade, near the region where the horseshoe vortex occurs. By increasing the wind angle of attack, for all building geometries, the CHTC distribution becomes asymmetric, where the maximum CHTC across the windward facade occurs near the upper most upstream corner of the windward facade. For the cases with $\theta \le 45^\circ$, the lowest values are observed in the lower part of the facade. For $\theta = 67.5^\circ$, however, the minimum CHTC values occur close to the upstream edge of the facade because of the dominance of flow separation and recirculation at this flow direction.

(b) The new CHTC expression

Three groups of simulations are performed to derive the new CHTC expression:

- The first group of simulations is performed to establish the expressions of forced surface-averaged CHTC as a function of reference wind speed U_{10} (or Re). The results show that for a given building geometry, the ratio $CHTC_{avg}/U_{10}^{0.84}$ is nearly independent of U_{10} for all reference wind directions. This indicates that the establishment of the relationship between CHTC, building height, and width and wind direction should only be performed for a single value of U_{10}, which saved time and computational cost.
- The second group of simulations is performed to establish the expression of forced surface-averaged CHTC as a function of wind speed, height and width of windward facade and wind direction. The results show that the ratio $CHTC_{avg}/U_{10}^{0.84}$ for the windward facades can be presented with high accuracy by a polynomial with windward building facade height and width and wind direction as parameters.
- The third group of simulations is performed to evaluate the out-of-sample accuracy of the expressions, indicating similarly high coefficients of determination as for the in-sample evaluation. The new CHTC expression is an analytical formula as a function of U_{10}, windward facade height, and building width, and wind direction that can easily be implemented in BES (building energy simulation) and BE-HAM (building envelope heat-air-moisture transfer) programs.
- The $CHTC_{avg}$ values obtained by the new CHTC expression and five commonly used CHTC expressions in BES tools are compared with the values directly obtained from the CFD simulations. The new expression provides a good agreement with the CFD results for different values of reference wind speed and wind direction. For the building with H = W = 10 m, for example, the deviation between the CFD results and the new expression results is about 0.8% for $\theta = 0^\circ$ and U_{10} = 1 m/s. This is about 2.8%, 1.4% and 0.3% for $\theta = 22.5^\circ$, 45° and 67.5°, respectively. For the other expressions, however, the deviations can be very large. For the building with H = W = 10 m, the use of the Nusselt-Jürges expression, for example, leads to a deviation of about 48% for $\theta = 0^\circ$ and U_{10} = 1 m/s. This deviation increases by increasing the wind direction and goes up to 93% for $\theta = 67.5^\circ$.

Future research on this topic will consist of:

- Evaluating the combined impacts of building geometry, wind speed and wind direction on the forced CHTC for facades other than the windward facade.
- Investigating the impact of different (small scale and large scale) surface roughness on the forced CHTC.
- Investigating the combined impacts of building geometry, wind speed, wind directions and urban surroundings on the mixed (forced and natural) CHTC, and establishing new expressions.

Acknowledgements

The authors gratefully acknowledge the partnership with ANSYS CFD. This work was sponsored by NWO Exacte Wetenschappen (Physical Sciences) for the use of supercomputer facilities, with financial support from the Nederlandse Organisatie voor Wetenschappelijk Onderzoek (Netherlands Organization for Scientific Research, NWO). Hamid Montazeri is currently a postdoctoral fellow of the Research Foundation – Flanders (FWO) at KU Leuven and is grateful for its financial support (project FWO 12M5316N).

References

[1] J. Allegrini, V. Dorer, J. Carmeliet, Analysis of convective heat transfer at building façades in street canyons and its influence on the predictions of space cooling demand in buildings, J. Wind Eng. Ind. Aerod. 104 (2012) 464–473.
[2] B. Blocken, Computational Fluid Dynamics for urban physics: importance, scales, possibilities, limitations and ten tips and tricks towards accurate and reliable simulations, Build. Environ. 91 (2015) 219–245.
[3] S. Bottillo, A. De Lieto Vollaro, G. Galli, A. Vallati, Fluid dynamic and heat transfer parameters in an urban canyon, Sol. Energy 99 (2014) 1–10.
[4] H. Montazeri, B. Blocken, D. Derome, J. Carmeliet, J.L.M. Hensen, CFD analysis of forced convective heat transfer coefficients at windward building facades: influence of building geometry, J. Wind Eng. Ind. Aerod. 146 (2015) 102–116.
[5] D.A. Vollaro, G. Galli, A. Vallati, CFD analysis of convective heat transfer coefficient on external surfaces of buildings, Sustainability 7 (2015), http://dx.doi.org/10.3390/su7079088.
[6] H. Montazeri, B. Blocken, New generalized expressions for forced convective heat transfer coefficients at building facades and roofs, Build. Environ. 119 (2017) 153–168.
[7] D.L. Loveday, A.H. Taki, Convective heat transfer coefficients at a plane surface on a full-scale building facade, Int. J. Heat Mass Tran. 39 (1996) 1729–1742.
[8] M.G. Emmel, M.O. Abadie, N. Mendes, New external convective heat transfer coefficient correlations for isolated low-rise buildings, Energy Build. 39 (2007) 335–342.
[9] B. Blocken, T. Defraeye, D. Derome, J. Carmeliet, High-resolution CFD simulations for forced convective heat transfer coefficients at the facade of a low-rise building, Build. Environ. 44 (2009) 2396–2412.
[10] R.N. Meroney, Studying the convective heat transfer from a building model with infrared camera techniques, ASME Winter Annual Meeting, December 10–15, 1978 San Francisco, California, May, 28 p, ASME Paper 78-WA/HT-58.
[11] T. Defraeye, J. Carmeliet, A methodology to assess the influence of local wind

conditions and building orientation on the convective heat transfer at building surfaces, Environ. Model. Software 25 (2010) 1813–1824.
[12] B. Blocken, J. Carmeliet, The influence of the wind-blocking effect by a building on its wind-driven rain exposure, J. Wind Eng. Ind. Aerod. 94 (2006) 101–127.
[13] B. Blocken, G. Dezsö, J. van Beeck, J. Carmeliet, Comparison of calculation models for wind-driven rain deposition on building facades, Atmos. Environ. 44 (2010) 1714–1725.
[14] T. Defraeye, B. Blocken, J. Carmeliet, Convective heat transfer coefficients for exterior building surfaces: existing correlations and CFD modelling, Energy Convers. Manag. 52 (2011) 512–522.
[15] M. Yazdanian, J.H. Klems, Measurement of the exterior convective film coefficient for Window in low-rise buildings, ASHRAE Transact. 100 (Part 1) (1994) 1087–1096.
[16] Y. Liu, D.J. Harris, Full-scale measurements of convective coefficient on external surface of a low-rise building in sheltered conditions, Build. Environ. 42 (2007) 2718–2736.
[17] W.H. McAdams, Heat Transmission, third ed., M CGraw Hill N. Y, New York-London, 1954.
[18] Guide Book A, Section A3, Chartered Institute of Building Services (CIBS), CIBS, London, 1979.
[19] J.A. Palyvos, A survey of wind convection coefficient correlations for building envelope energy systems' modeling, Appl. Therm. Eng. 28 (2008) 801–808.
[20] M. Mirsadeghi, D. Cóstola, B. Blocken, J.L.M. Hensen, Review of external convective heat transfer coefficient models in building energy simulation programs: implementation and uncertainty, Appl. Therm. Eng. 56 (2013) 134–151.
[21] W. Jürges, Der Wärmeübergang an einer ebenen Wand, Druck und Verlag von R. Oldenbourg, 1924.
[22] M.K. Chyu, V. Natarajan, Local heat mass-transfer distributions on the surface of a wall-mounted cube, J. Heat Transf.-Trans. ASME 113 (1991) 851–857.
[23] V. Natarajan, M.K. Chyu, Effect of flow angle-of-attack on the local heat/mass transfer from a wall-mounted cube, Trans. ASME J. Heat Transf. 116 (1994) 552–560.
[24] E.R. Meinders, K. Hanjalic, R.J. Martinuzzi, Experimental study of the local convection heat transfer from a wall-mounted cube in turbulent channel flow, Trans. ASME J. Heat Transf 121 (1999) 564–573.
[25] H. Nakamura, T. Igarashi, T. Tsutsui, Local heat transfer around a wall-mounted cube in the turbulent boundary layer, Int. J. Heat Mass Tran. 44 (2001) 3385–3395.
[26] S. Murakami, Comparison of various turbulence models applied to a bluff body, J. Wind Eng. Ind. Aerod. 46 (1993) 21–36.
[27] B. Blocken, 50 years of computational wind engineering: past, present and future, J. Wind Eng. Ind. Aerod. 129 (2014) 69–102.
[28] S. Iousef, H. Montazeri, B. Blocken, P.J.V. van Wesemael, Impact of Exterior Convective Heat Transfer Coefficient Models on the Energy Demand Prediction of Buildings with Different Geometry, (2018) under review.
[29] E.R. Meinders, T.H. Van Der Meer, K. Hanjalic, Local convective heat transfer from an array of wall-mounted cubes, Int. J. Heat Mass Tran. 41 (1998) 335–346.
[30] E.R. Meinders, K. Hanjalić, Vortex structure and heat transfer in turbulent flow over a wall-mounted matrix of cubes, Int. J. Heat Fluid Flow 20 (1999) 255–267.
[31] E.R. Meinders, K. Hanjalić, Experimental study of the convective heat transfer from in-line and staggered configurations of two wall-mounted cubes, Int. J. Heat Mass Tran. 45 (2002) 465–482.
[32] H. Nakamura, T. Igarashi, T. Tsutsui, Local heat transfer around a wall-mounted cube at 45 to flow in a turbulent boundary layer, Int. J. Heat Fluid Flow 24 (2003) 807–815.
[33] M. Yaghoubi, E. Velayati, Undeveloped convective heat transfer from an array of cubes in cross-stream direction, Int. J. Therm. Sci. 44 (2005) 756–765.
[34] K.-C. Wang, R.-T. Chiou, Local mass/heat transfer from a wall-mounted block in rectangular channel flow, Heat Mass Tran. 42 (2006) 660–670.
[35] T. Defraeye, B. Blocken, J. Carmeliet, CFD analysis of convective heat transfer at the surfaces of a cube immersed in a turbulent boundary layer, Int. J. Heat Mass Tran. 53 (2010) 297–308.
[36] J. Liu, M. Heidarinejad, S. Gracik, J. Srebric, The impact of exterior surface convective heat transfer coefficients on the building energy consumption in urban neighborhoods with different plan area densities, Energy Build. 86 (2015) 449–463.
[37] E.R. Meinders, Experimental Study of Heat Transfer in Turbulent Flows over Wall Mounted Cubes, PhD thesis Technische Universiteit Delft, 1998.
[38] H.M. Künzel, K. Kiessl, Calculation of heat and moisture transfer in exposed building components, Int. J. Heat Mass Tran. 40 (1996) 159–167.
[39] B. Blocken, J. Carmeliet, A review of wind-driven rain research in building science, J. Wind Eng. Ind. Aerod. 92 (2004) 1079–1130.
[40] H. Janssen, B. Blocken, J. Carmeliet, Conservative modelling of the moisture and heat transfer in building components under atmospheric excitation, Int. J. Heat Mass Tran. 50 (2007) 1128–1140.
[41] Ansys Inc, Ansys Fluent 12.0 – Theory Guide, (2009) USA: Lebanon.
[42] T.-H. Shih, W.W. Liou, A. Shabbir, Z. Yang, J. Zhu, A new k-ε eddy viscosity model for high Reynolds number turbulent flows, Comput. Fluids 24 (1995) 227–238.
[43] M. Wolfshtein, The velocity and temperature distribution in one-dimensional flow with turbulence augmentation and pressure gradient, Int. J. Heat Mass Tran. 12 (1969) 301–318.
[44] S. Iousef, H. Montazeri, B. Blocken, P.J.V. van Wesemael, On the use of non-conformal grids for economic LES of wind flow and convective heat transfer for a wall-mounted cube, Build. Environ. 119 (2017) 44–61.
[45] Z.-X. Hu, G.-X. Cui, Z.-S. Zhang, Numerical study of mixed convective heat transfer coefficients for building cluster, J. Wind Eng. Ind. Aerod. 172 (2018) 170–180.
[46] B. Blocken, J. Carmeliet, T. Stathopoulos, CFD evaluation of wind speed conditions in passages between parallel buildings—effect of wall-function roughness modifications for the atmospheric boundary layer flow, J. Wind Eng. Ind. Aerod. 95 (2007) 941–962.
[47] B. Blocken, T. Stathopoulos, J. Carmeliet, CFD simulation of the atmospheric boundary layer: wall function problems, Atmos. Environ. 41 (2007) 238–252.
[48] W. Rodi, Comparison of LES and RANS calculations of the flow around bluff bodies, J. Wind Eng. Ind. Aerod. 69 (1997) 55–75.
[49] Y. Tominaga, A. Mochida, S. Murakami, S. Sawaki, Comparison of various revised k– ε models and LES applied to flow around a high-rise building model with 1: 1: 2 shape placed within the surface boundary layer, J. Wind Eng. Ind. Aerod. 96 (2008) 389–411.
[50] N. Antoniou, H. Montazeri, H. Wigo, M.K.-A. Neophytou, B. Blocken, M. Sandberg, CFD and wind-tunnel analysis of outdoor ventilation in a real compact heterogeneous urban area: evaluation using “air delay”, Build. Environ. 126 (2017) 355–372.
[51] Y. Tominaga, A. Mochida, R. Yoshie, H. Kataoka, T. Nozu, M. Yoshikawa, T. Shirasawa, AIJ guidelines for practical applications of CFD to pedestrian wind environment around buildings, J. Wind Eng. Ind. Aerod. 96 (2008) 1749–1761.
[52] J. Franke, A. Hellsten, H. Schlünzen, B. Carissimo, Best Practice Guideline for the CFD Simulation of Flows in the Urban Environment. COST Action 732: Quality Assurance and Improvement of Microscale Meteorological Models, (2007).
[53] R. Ramponi, B. Blocken, CFD simulation of cross-ventilation for a generic isolated building: impact of computational parameters, Build. Environ. 53 (2012) 34–48.
[54] A. Rezaeiha, H. Montazeri, B. Blocken, Towards accurate CFD simulations of vertical axis wind turbines at different tip speed ratios and solidities: guidelines for azimuthal increment, domain size and convergence, Energy Convers. Manag. 156 (2018) 301–316.
[55] T. van Hooff, B. Blocken, Coupled urban wind flow and indoor natural ventilation modelling on a high-resolution grid: a case study for the Amsterdam ArenA stadium, Environ. Model. Software 25 (2010) 51–65.
[56] J. Wieringa, Updating the Davenport roughness classification, J. Wind Eng. Ind. Aerod. 41 (1992) 357–368.
[57] B. Ničeno, A.D. Dronkers, K. Hanjalić, Turbulent heat transfer from a multi-layered wall-mounted cube matrix: a large eddy simulation, Int. J. Heat Fluid Flow 23 (2002) 173–185.
[58] M. Popovac, Modelling and Simulation of Turbulence and Heat Transfer in Wall-bounded Flows, PhD thesis. Technische Universiteit Delft, 2006.
[59] H. Nakamura, T. Igarashi, T. Tsutsui, Local heat transfer around a wall-mounted cube at 45° to flow in a turbulent boundary layer, Int. J. Heat Fluid Flow 24 (2003) 807–815.
[60] J.W. Mitchell, Heat transfer from spheres and other animal forms, Biophys. J. 16 (1976) 561–569.
[61] G.N. Walton, Thermal Analysis Research Program Reference Manual, NBSSIR 83–2655, National Bureau of Standards (1983).
[62] M. Casey, T. Wintergerste, Best Practice Guidelines: ERCOFTAC Special Interest Group on“ Quality and Trust in Industrial CFD”, ERCOFTAC (2000).
[63] P. Tucker, A. Mosquera, NAFEMS Introduction to Grid and Mesh Generation for CFD, NAFEMS CFD Working Group, 2001, p. 56 R0079.
[64] F.B. Rowley, A.B. Algren, J.L. Blackshaw, Surface conductances as affected by air velocity, temperature and character of surface, ASHRAE Trans. 36 (1930) 429–446.
[65] R.J. Cole, N.S. Sturrock, The convective heat exchange at the external surface of buildings, Build. Environ. 12 (1977) 207–214.
[66] T. Stathopoulos, X. Zhu, Wind pressures on building with appurtenances, J. Wind Eng. Ind. Aerod. 31 (1988) 265–281.
[67] S. Murakami, Computational wind engineering, J. Wind Eng. Ind. Aerod. 36 (1990) 517–538.
[68] I. Chand, P.K. Bhargava, N.L.V. Krishak, Effect of balconies on ventilation inducing aeromotive force on low-rise buildings, Build. Environ. 33 (1998) 385–396.
[69] H. Montazeri, B. Blocken, CFD simulation of wind-induced pressure coefficients on buildings with and without balconies: validation and sensitivity analysis, Build. Environ. 60 (2013) 137–149.
[70] H. Montazeri, B. Blocken, W.D. Janssen, T. van Hooff, CFD evaluation of new second-skin facade concept for wind comfort on building balconies: case study for the Park Tower in Antwerp, Build. Environ. 68 (2013) 179–192.
[71] S. Omrani, V. Garcia-Hansen, B.R. Capra, R. Drogemuller, On the effect of provision of balconies on natural ventilation and thermal comfort in high-rise residential buildings, Build. Environ. 123 (2017) 504–516.
[72] H. Montazeri, F. Montazeri, CFD simulation of cross-ventilation in buildings using rooftop wind-catchers: impact of outlet openings, Renew. Energy 118 (2018) 502–520.
[73] J. Allegrini, V. Dorer, T. Defraeye, J. Carmeliet, An adaptive temperature wall function for mixed convective flows at exterior surfaces of buildings in street canyons, Build. Environ. 49 (2012) 55–66.
[74] J. Liu, J. Srebric, N. Yu, Numerical simulation of convective heat transfer coefficients at the external surfaces of building arrays immersed in a turbulent boundary layer, Int. J. Heat Mass Tran. 61 (2013) 209–225.
[75] N. Nazarian, J. Kleissl, Realistic solar heating in urban areas: air exchange and street-canyon ventilation, Build. Environ. 95 (2016) 75–93.